

Extracting dualband antenna response from UWB based on current distribution analysis

Mahmood T. Yassen¹, Mohammed R. Hussan², Ali J. Salim², Hussam Alsaedi², Jawad K. Ali²

¹ Department of Electrical Engineering, University of Technology, Iraq

² Department of Communication Engineering, University of Technology, Iraq

ABSTRACT

An entirely new design approach has been employed to create the printed dualband monopole antenna that was the subject of this investigation. The printed monopole antenna construction is the primary component of the suggested design. CPW transmission lines with 50 Ohm impedance and a relative dielectric constant of 4.6 were used to power the antennas, which were housed in thin substrates with thicknesses of 1.6 millimeters (mm). In this study, the antennas discussed were modeled and analyzed by Computer Simulation Technique (CST) simulator. Using fractal structures on the radiating element of a dualband antenna can improve the resonance of the antenna as well as the coupling of the resonating bands that emerge from the resonance.

Keywords: Multiband antenna, UWB antenna, Microstrip antenna, Fractal geometry, Current distribution

Corresponding Author:

Jawad K. Ali
Department of Communication Engineering
University of Technology - Iraq
Assinaa Street, Baghdad, Iraq
E-mail: jawengin@yahoo.com

1. Introduction

The need for dual-band and compact antennas is increasing as the number of wireless communication services and related applications continues to grow. A multitude of different types of communication systems can be developed by telecom operators and equipment manufacturers. The ability to work across a broad band of frequencies is shared by all of them. In order to provide service to its customers, each system must be equipped with an antenna under operating frequency band. However, this method is both inefficient and expensive, as evidenced by the fact that each system had only one antenna at one point in time. Antennas with dual or multiple bands are essential due to the wide variety of communication technologies now available. It is feasible to provide dual-band functionality in a variety of methods by combining printed and microstrip antennas in different configurations. Among the many sorts of design approach that fall under this wide category are: geometric, organic, and narrative.

It's the most prevalent design in the world of dual-band microstrip antennas since it is so simple to implement. First, the rectangular patch has two orthogonal dimensions, and the first resonance of these dimensions is used to construct a single patch. If the patch's two orthogonal sides are also orthogonal, the frequency ratio will be the same on both. This approach, on the other hand, has the obvious drawback of activating two polarizations at the same time. As long as the polarization requirements aren't critical, this basic approach can be useful.

It's called the "second form" of design when a single patch has reactive loading, such as capacitance or varactory [2, 3], notches [4, 5], or PIN diode stabs. It is possible to use both external (slots 8-12) and integrated slots (slots 13-15).

Patches with reactive loading can be modified to make a radiation pattern of the higher-order mode highly comparable to a radiation pattern of a fundamental frequency. It is also possible to produce dual-band functioning by combining dual or more radiating components on a similar substrate, each is capable of maintaining high currents and radiation at the resonance." Patches having a large number of substrates and layers [16] are also included in this category. Dual polarization indicates that these antennas have the same polarization for both frequencies, which is a significant advantage. The same multilayer structures that are used to bridge the frequency gap are as well utilized to increase a bandwidth of a single band antenna.

Those having fractal geometry for dual-band operation are included in this category of antennas. It is feasible to reduce the size of antennas as well as other microwave circuits and components by employing fractal geometry techniques. Fractal structures have been used to construct a variety of space-filling filters for a wide range of applications [19-32], including but not limited to: Consequently, with the assistance of other techniques, it may be able to construct tiny dual- and multi-band systems. As a result, the SIR has been used successfully in the past to accomplish this objective. The features of fractal geometry allow for the use of fractal-shaped antenna structures to produce dual-band behavior, which is another technique that has seen widespread application. It is possible to leverage the space-filling property of fractal geometry [41, 42] to reduce the size of the antenna while simultaneously boosting its responsiveness [43, 44]. High nonharmonic resonant frequencies can be achieved by the use of geometric self-similarity in dual and multi-band antenna designs. Compared to non-fractal Euclidean geometries, fractal antennas possess better-quality impedance and voltage standing wave ratio (VSWR) performance due to their compact physical area.

These findings indicate a novel technique to the fabrication of printed dualband antennas that is worth mentioning. The UWB response is used to derive the dual-band resonant behavior of the system. It is necessary to analyze the current distributions on the antenna component surfaces under a variety of frequencies in order to determine their contributions to the formation of resonances. It is therefore possible to achieve dual-band resonance behavior by increasing the currents at the necessary resonance frequencies while utilizing an antenna that has been modified in this manner. Almost any UWB antenna has a wide range of resonant bands, and the technique projected takes advantage of this trait to adapt the response to the resonant behavior of any specific antenna. The design of antennas has been suggested as a contributing factor to the occurrence of various resonance frequencies. These frequencies can be used to inspect the surface current distributions of the antenna for any anomalies and to determine whether or not the antenna is functioning properly. It is possible to modify the antenna's construction in order to achieve dual-band functionality, which results in the antenna's dual-band characteristics.

2. The Square Printed Monopole UWB Antenna

With commercial usage of the UWB spectrum, 3.1-10.6 GHz, ratified by the U.S. Federal Communications Commission (FCC), academic and industrial interest in this technology has grown. Antenna downsizing and bandwidth increase are both critical antenna engineering strategies. To meet the UWB resonance in many applications, numerous researchers have developed new approaches for designing compact size antennas with broad bandwidth performance.

2.1. The UWB Antenna topology

The printed square UWB monopole antenna layout shown in Figure 1 is a projected design. Figure 1 depicts the front perspective of the radiator-containing structure, as well as the CPW feed mechanism used to power the radiator. The projected antenna's approximate overall dimensions (including the substrate) are 43 by 40 millimeters, with a printed layer of glass epoxy (FR4) on top that is projected to be 16 mm thick and have a relative permittivity of 4.6 millimeters on the top surface. The radiating patch is comprised of a square shape with $(W_p L_p)$ and has been excited by a 50 Hz CPW-feeding approach to produce heat. The feed line has the following dimensions: $(W_f L_f)$, the gap between a feeder and the ground plane is (g_1) , and the spacing between the ground plane and a radiator is (g_2) (g_2) . Slots had been cut from the higher and bottom corners of a patch in a stepwise fashion, with the measurements W_{st1} L_{st1} , W_{st2} L_{st2} , besides W_{st3} L_{st3} being the first, second, and third slots, respectively.

$(W_{gp} \times L_{gp})$ is the ground plane dimension on both sides of the feeder on both sides. The resulting optimum parameter values are shown in Table 1 below. It is critical to emphasize that all of the dimensions are included (mm).

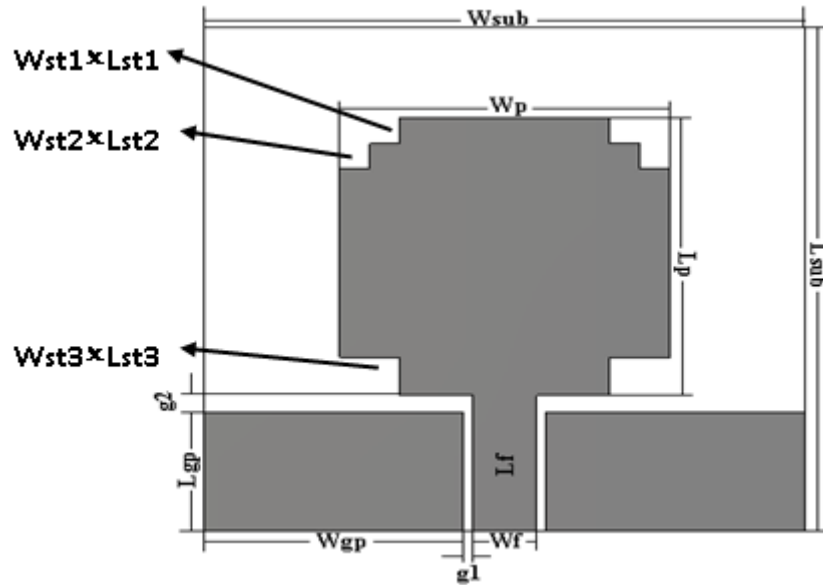


Figure 1. The envisioned UWB antenna with a printed monopole

Table 1. The characteristics of the antennas presented in this paper as depicted in Figure 1

Antenna Components	Symbols and their values of the proposed antenna in (mm)
Radiator	$W_p = 22, L_p = 22$
Upper Steps	$W_{st1} = 2, L_{st1} = 2, W_{st2} = 2, L_{st2} = 2$
Lower Steps	$W_{st3} = 4, L_{st3} = 3$
Feed Line	CPW, $W_f = 4.2, L_f = 10.79, g_1 = 0.66, g_2 = 1.29$
Ground plane	$W_{gp} = 17.24, L_{gp} = 9.5$
Substrate	$W_{sub} = 40, L_{sub} = 43, h = 1.6$

It has been demonstrated that in a projected square printed monopole UWB antenna, the patch length (L_p) based on guided wavelength is a significant determinant in performance.

$$\lambda_g = \frac{\lambda_0}{\sqrt{\epsilon_{reff}}} \tag{1}$$

where ϵ_{reff} refers to a magnitude of effective dielectric constant, with a feeder width of W_f to a substrate height of W_f/h and the following formula::

$$\epsilon_{reff} = \frac{\epsilon_r + 1}{2} + \frac{\epsilon_r - 1}{2} \left(\frac{1}{\sqrt{1 + 12h/W_f}} \right) \tag{2}$$

The (f_L) that stands for lower resonant frequency, based on radiating patch length (L_p) can be evaluated as below:

$$f_L \approx \frac{C_0}{2(L_p + \Delta L)\sqrt{\epsilon_{reff}}} \tag{3}$$

where C_o represents a light speed in free space, ΔL stands for an incremental length based on fringing for a field at respective edges:

$$\Delta L \approx W_{st1} + W_{st3} \quad (4)$$

Consequences of the suggested monopole UWB antenna were depicted in Figures 2 -3. Figure 2 depicts an antenna's S11 response to 50 broadcasts at a frequency range simulated to span from 1 to 11 GHz. 2.8 to 10.65 GHz is a wide operating frequency range for the projected antenna, which has outstanding UWB properties. The square patch length L_p determines the lower resonance frequency of 2.8 GHz and is dictated by (3). These four pole frequencies are 3.77 GHz, 5.82 GHz, 7.93 GHz, 9,74% and S11 values of -37.41dB, 22.3dB and 18dB, respectively, at these four frequencies. The antenna responds to UWB frequencies because of these pole frequencies. Fig. 2 shows that S11's value is significantly below the -10 dB threshold within the UWB frequency range.

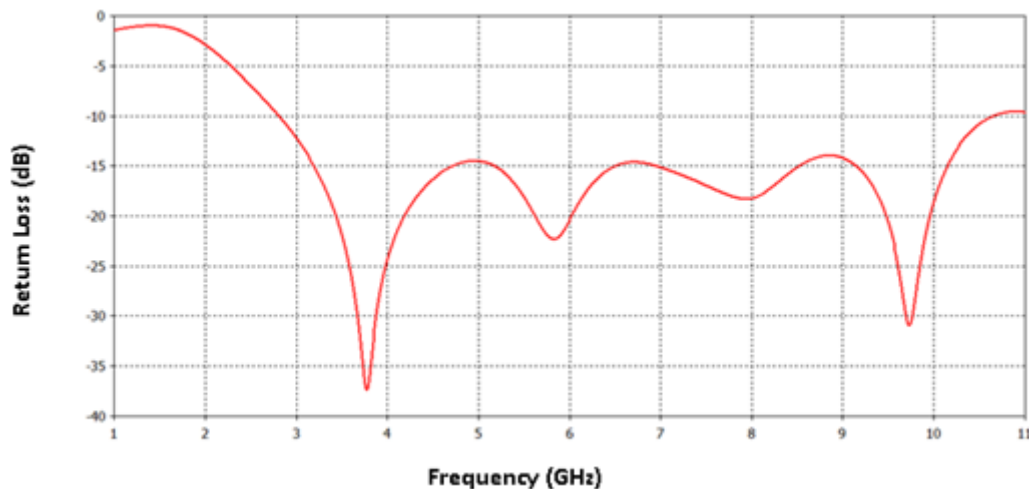


Figure 2. The simulated S11 coefficient for a projected printed monopole UWB antenna

A current distribution representation for the planned UWB antenna based on spectrum of resonance frequencies is depicted in Figure 3. At the lower resonance frequency of 2.8 GHz (Fig. 3a) and the 1st pole frequency of 3.77 GHz (Fig. 3b), the current concentration at the respective side lengths can be used to determine how the current is dispersed in these frequencies. Figure 3: Current concentration at the respective side lengths Higher and lower steps, as well as lower steps and radiator side length, are shown to have a direct effect on radiation at resonance frequencies of 5.82 and 7.93 GHz in figures 3(c) and (d). Huge currents are flowing through the radiator at the 4th pole of the 9.74 GHz resonance frequency and at the highest resonant frequency of 10.65 GHz, which are both near the fourth pole of the resonance frequency. The current is concentrated in these places due to the top width and internal lengths of the ground plane being taken into consideration. Feed lines continue to flow at all resonant frequencies throughout the length of the line.

2.2. The steps impact on a resonance of the projected UWB antenna

One of the most essential qualities of the UWB antenna is its ability to operate inside the permitted spectrum band by the Federal Communications Commission. The bandwidth of UWB antennas can be enhanced in a variety of methods, with slots being the most commonly used method by far. The paper in [48] shows a proposed antenna with slots in the patch's top and lower corners, which are based on square and rectangular cuts, to ensure wideband matching for a transmission system with a radiator.

Figure 4 displays the outcomes of the acts that have taken place thus far. It has been discovered that inserting these techniques in order to obtain a wide bandwidth and suitable impedance matching in order to optimize antenna radiation efficiency is the most successful method.

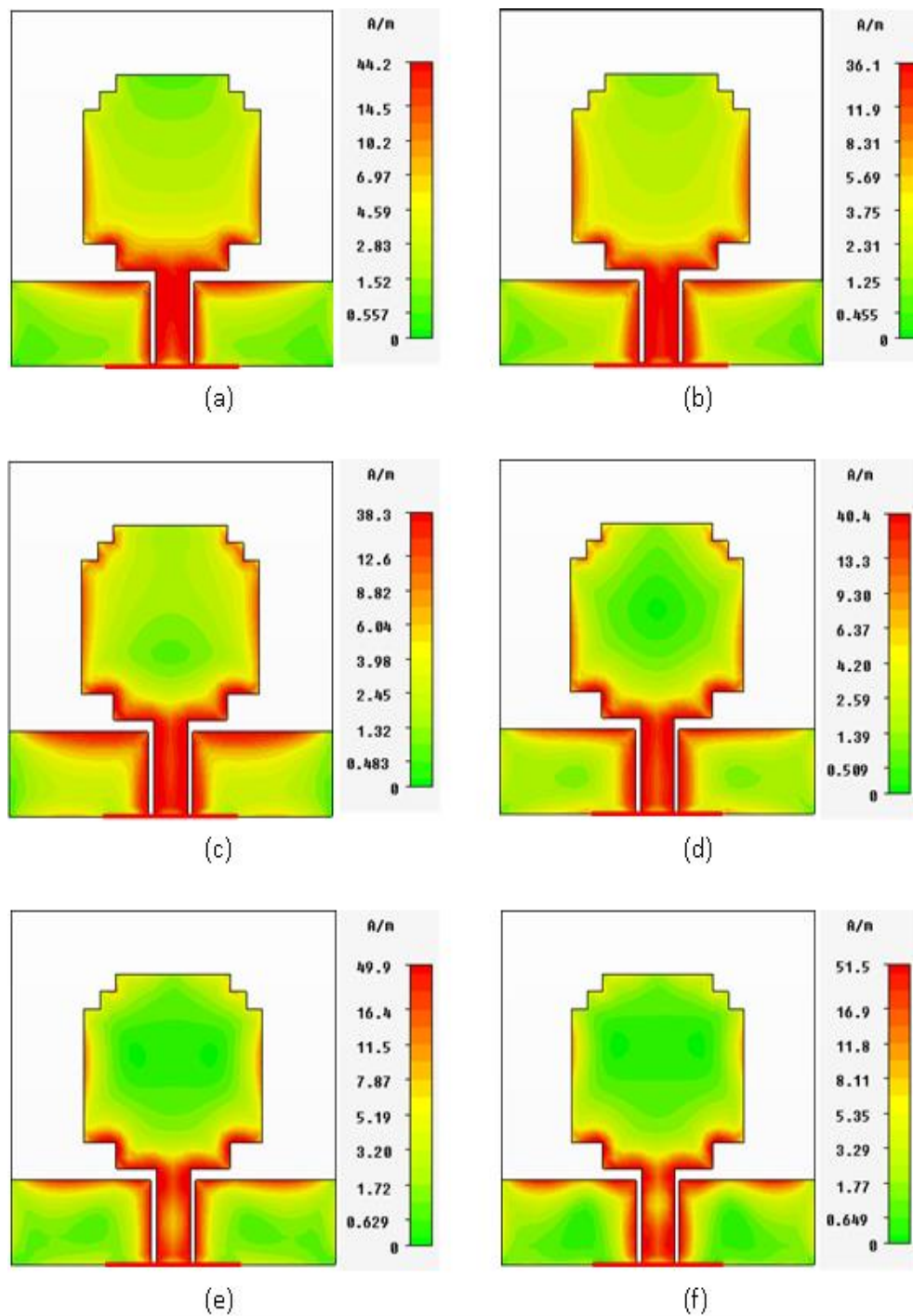


Figure 3. Surface simulations of the proposed UWB antenna at frequencies of (a) 2.8 GHz, (b) 3.77 GHz, (c) 5.82 GHz, (d) 7.93 GHz, (e) 9.74 GHz, and (f) 10.65 GHz

3. Variations on the UWB antenna components

The surface current distribution based on resonant frequencies of the projected antenna have been used to modify a square printed monopole antenna with a UWB resonance to display dual-band resonant behavior. The patch needs to be modified first. The second is a change to the ground plane and feed line, which makes use of the same substrate qualities and feeding approach as the projected UWB antenna.. Patch and ground plane sites that generate UWB resonance at higher frequencies are intended to be removed by these changes. Additionally, boost UWB resonance zones that also resonate at lower frequencies by increasing the current.

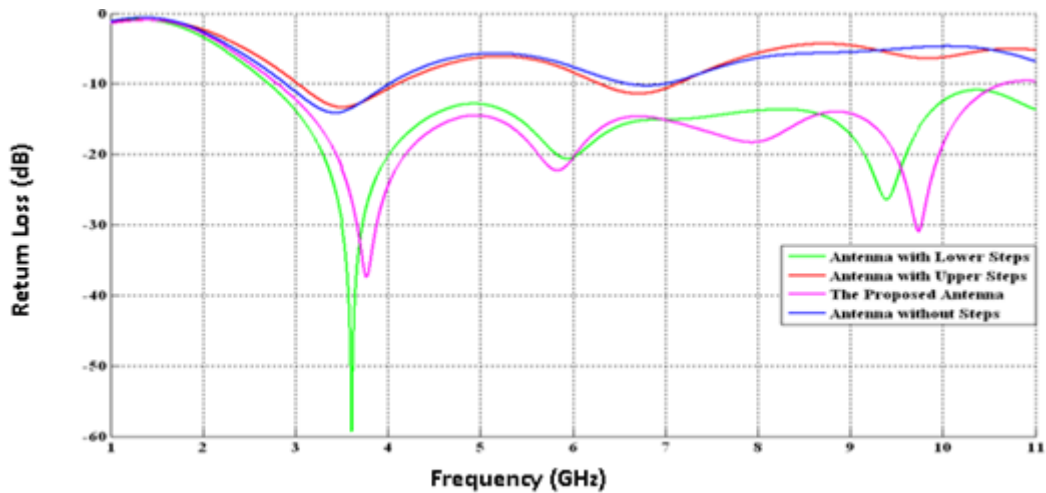


Figure 4. Impact of steps on a resonant frequency for a projected UWB antenna

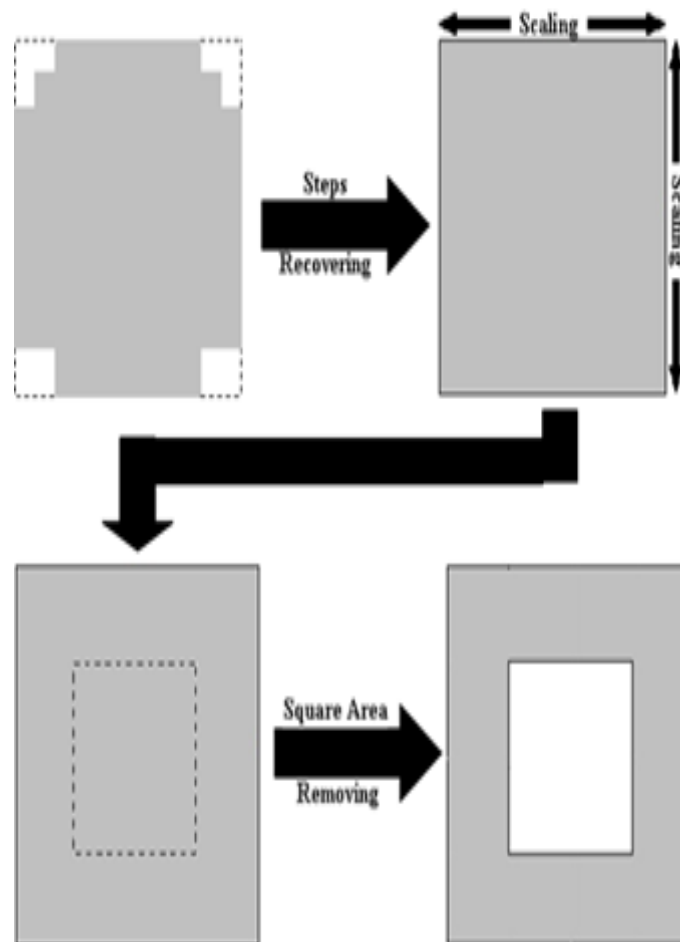


Figure 5. Antenna radiating element transformations

Fig. 5 explains the antenna patch change. There are dual bands with $S_{11} \leq -10$ dB once the steps have been recovered, as shown in Fig. 4. For reducing the lower resonance frequency, the patch size are increased in the second step. Fig. 3 shows that the patch's central area has no correlation to the lower resonance frequency. Another step is to cut out a portion of patch in order to boost current flow in critical lower resonance frequency zones.

An antenna ground plane and feeder adjustment in Fig. 6 is simplified. Ground plane area reduction and feed line width reduction are used to improve the bandwidth of the high resonance band achieved after patch modification by increasing the impedance matching. As can be seen in Figure 3(c), there is a significant quantity of current flowing down the feed line's internal lengths and the ground plane's top breadth. Its purpose is to enhance the overall current in this region, hence enhancing the creation of resonance frequencies.

4. The subsequent antenna design

It is important that the dualband antenna generated by modifying the proposed UWB antenna has a reasonable bandwidth, gain, and radiation properties to meet the requirements of wireless communication communities. In order to determine the antenna performance, the CST software is employed. The structure, design, and performance assessment of the antenna are covered in further depth in the subsequent sections.

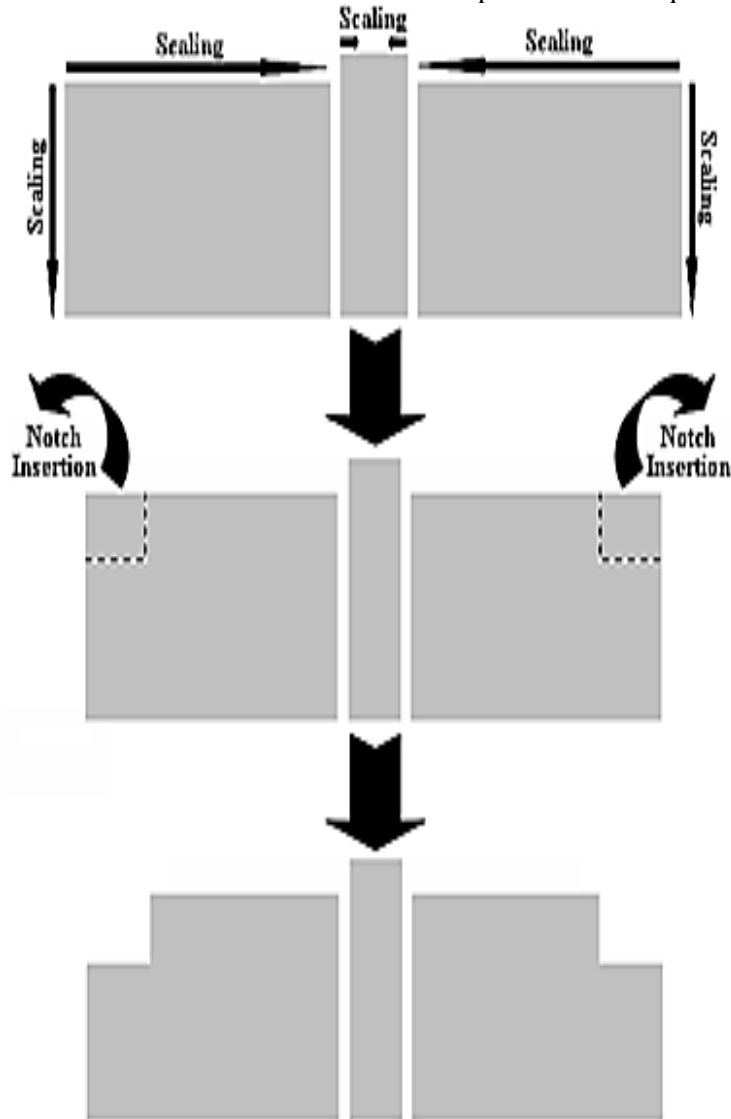


Figure 6. Antenna feeder and ground plane changes

4.1. The topology of antenna

After assembly, the frontal antenna shape is shown in Figure 7. It is necessary to employ the feed method of a UWB antenna in order to excite a square radiator with an outward dimension of ($W_p \times L_p$) and an internal dimension of ($W_s \times L_s$). A shave has been performed on each of the ground plane's upper corners in order to produce two rectangular holes. Antenna parameters are summarized in Table 2 and illustrated in Figure 7 with their altered size.

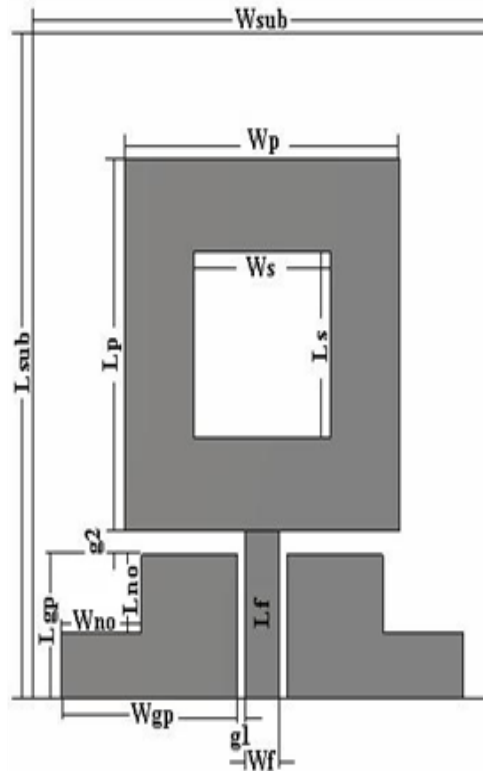


Figure 7. The resultant square printed monopole dualband antenna

Table 2. Details of the modified parameters of the resulting dual-band antenna, as labeled in Figure 7

Antenna Components	Symbols and their values of the proposed antenna in (mm)
Radiator	$W_p = 24, L_p = 24$
Inner Square Slot	$W_s = 12, L_s = 12$
Feed Line	CPW, $W_f = 3, L_f = 10.79, g_1 = 0.66, g_2 = 1.59$
Ground plane	$W_{gp} = 15.34, L_{gp} = 9.2$
Ground Plane Notch	$W_{no} = 7, L_{no} = 5$
Substrate	$W_{sub} = 40, L_{sub} = 43, h = 1.6$

Wireless communication applications will benefit from the square printed monopole dual band antenna. The radiator's internal slot length (L_s) and roughly 77% of its exterior length (L_p) were discovered to have a direct impact on the lower resonant frequency as effective length (L_{eff}) based on a guided wavelength after modification operations and dimensions scaling. In this case, the length of L_{eff} can be expressed as follows:

$$L_{eff} = L_s + 0.77L_p \tag{5}$$

The lower resonant frequency, (f_{L1}), based on radiating element length (effective length) can be evaluated by:

$$f_{L1} \approx \frac{C_o}{2L_{eff} \sqrt{\epsilon_{reff}}} \tag{6}$$

The light speed in open space is represented by the symbol C_o .

4.2. The subsequent antenna performance

The consequences of the square monopole dualband antenna are depicted in Figures 8-12, which illustrate that they were obtained. Figure 8 explains the response of the antenna's input reflection coefficient over a frequency range of one to ten gigahertz, as determined using simulation.

The performance of this antenna on both bands is extremely obvious. Dual resonant frequency bands (for $S_{11} < -10$ dB) may be found: a lower resonant band from 2.64 to 3.55GHz with a core frequency of 3.08GHz for -14.8dB S_{11} , besides the higher resonant band from 5.55–6.85GHz with a central frequency of 5.98GHz for 29.97dB S_{11} . This antenna has a frequency ratio (ω_1/ω_2) of 0.52, which is a good value. We were able to examine the surface currents and illustrate them in Figure 9 thanks to the modeling tool. Figure 9(a) depicts the antenna surface current at the lower resonant band's center frequency of 3.08 GHz; the antenna's surface current is concentrated in the radiator's bottom breadth and some of the radiator's internal slot lengths. Figure 9(b) depicts a surface current for the antenna at the central frequency of 5.98 GHz, which is focused at the radiator's dual upper inner corners along with a lower breadth of the antenna's radiator. A feed line has been the primary conduit for the vast majority of the current flowing at the frequencies that have been previously stated.

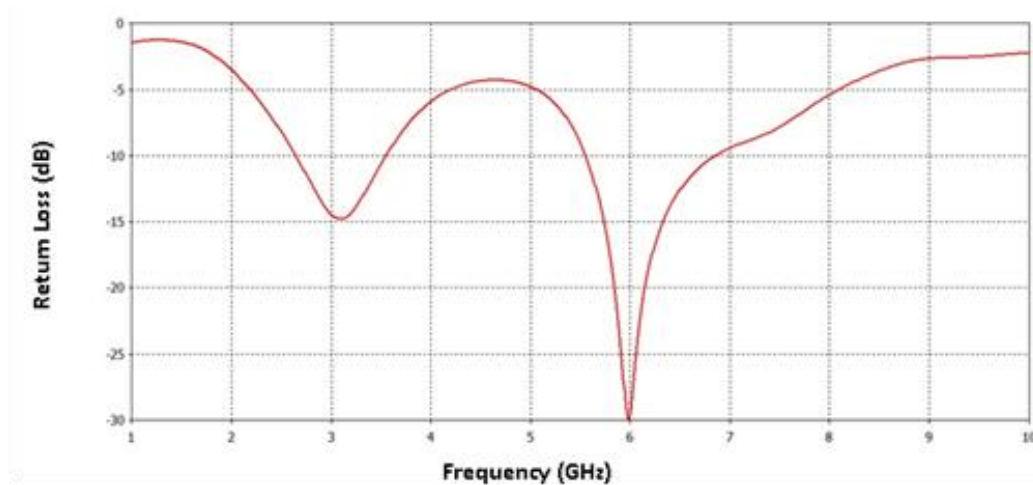


Figure 8. Antenna's simulated S_{11} parameter for the square printed dualband monopole antenna

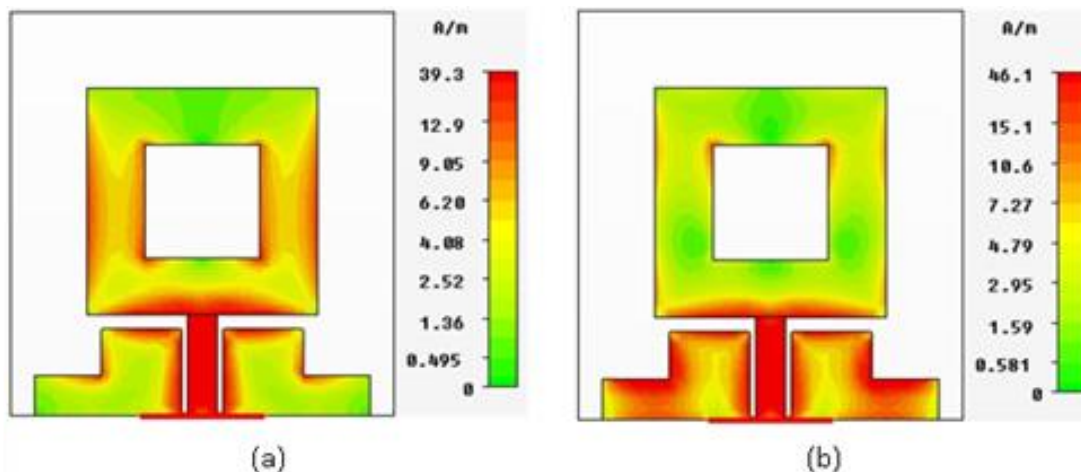


Figure 9. Surface simulations of the printed monopole dual-band antenna's current distribution at (a) 3.08 GHz and (b) 5.98 GHz

Fairfield radiation patterns based on overall electric field in the x-y plane, x-z plane, in addition to the y-z plane at the central frequencies of dual bands are depicted in Fig. 10. The radiation patterns at 3.08 GHz are shown in Fig. 10(a). A 16.1 dB major lobe is located at (167°) in the x-y plane ($\theta = 90^\circ$), and its 3 dB angular breadth is located at (90.4°) . Its magnitude is 17.4dB V/m and its direction is north-northeast (north-northeast) (180°) . While in the y-z plane ($\phi = 90^\circ$), the main lobe value has been 17.5 dB, the main lobe direction has been 173° ,

along with an angular breadth (3 dB) is (79°). At 5.98 GHz, radiation patterns are seen in Fig. 10(b). Using the x-y coordinate system ($\phi = 90^\circ$), the major lobe level is -4.2 dB, the main lobe angle is (126°), the three-dimensional angular breadth (3 dB) is 38.5°. There are three primary lobes: one in the (138°) direction, one in the (0°) x-z plane, besides one in (0°) the angular width (3 dB) (62.1°). As opposed to this, the main lobe level in the y-z plane ($\phi = 90^\circ$) measures 16.5 decibels (dB), the main lobe direction is (142°), the 3 decibel angular breadth is (44.4°), and sidelobe level is -1.7 dB.

Fig. 11 depicts the antenna's simulated three-dimensional directivity radiation patterns as far as radiation attributes go. While the lower band directivity at 3.08 GHz is reported in Figure 11(a) to be 2.66 dBi, the upper band directivity is shown to be 5.27 dBi in the same figure (b).

Based on Fig. 12, the maximum gain magnitudes in the two bands have been calculated. Fig. 12(a) shows a peak gain of 1.59 dBi in the lower frequency region. Fig. 12(b) shows the gain vs frequency for the upper band, with a maximum gain of 6.14 dBi.

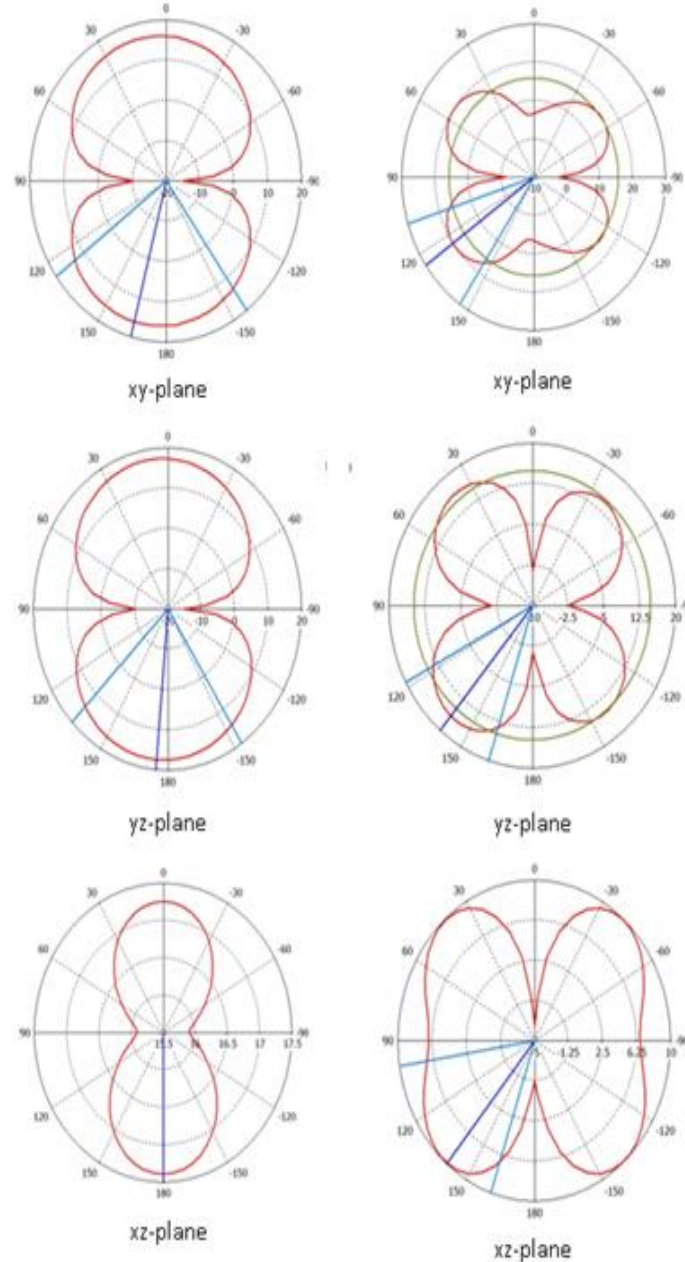


Figure 10. Far-field radiation patterns of the final square printed monopole dual-band antenna modeled from its total electric field at (a) 3.08 GHz, and (b) 5.98 GHz

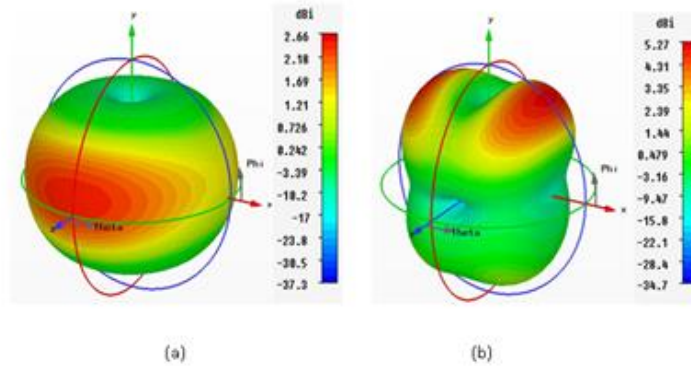


Figure 11. Simulation of the resulting dual-band antenna's 3D directivity at (a) 3.08 GHz, and (b) 5.98 GHz

5. Dualband antenna resulting from using fractal geometry

The resonance of the consequential dualband antenna was improved using the Minkowski fractal from the first, second, and third iterations. The Minkowski space-filling fractal structure is shown in Fig. 13 and will be applied to the antenna construction that results. A Euclidean line is shown in Fig. 13(a) as the initiator. The center part of the initiator will be replaced by the generator. As illustrated at the bottom of Fig. 13, each segment has a length equal to one-third that of the initiator's. In Fig. 13(b), the generating structure has five straight segments, each of which is replaced by a generator. Infinite repetitions of this iterative generation process are possible. Final product has an indefinitely complex underlying structure that can't be differentiated at any time.

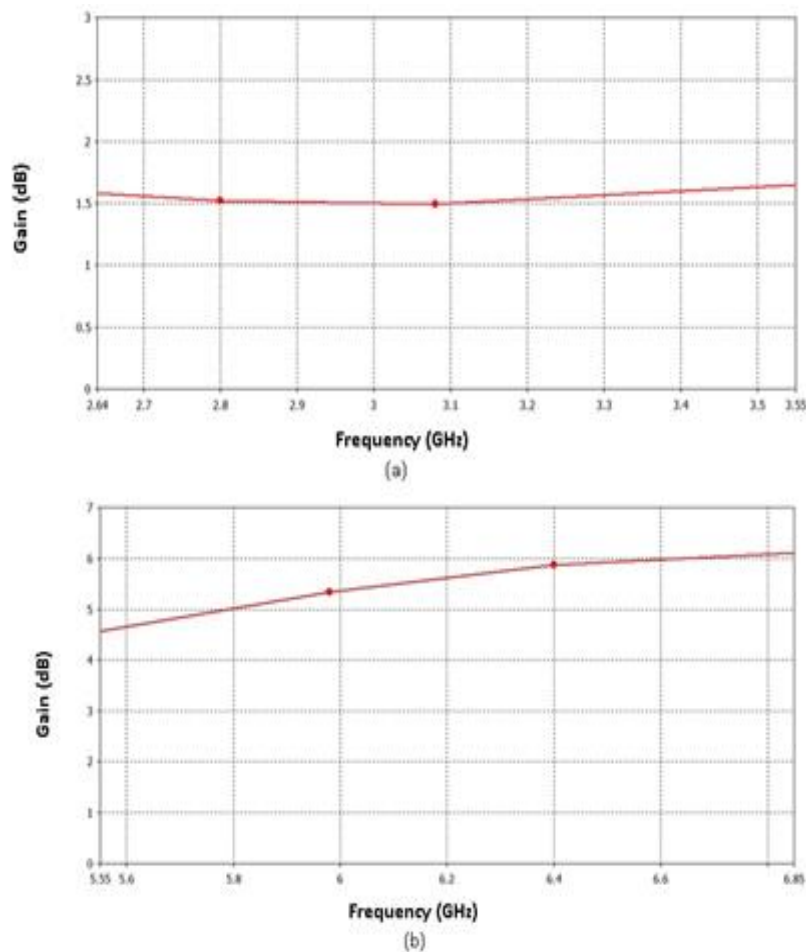


Figure.12. Simulation of peak gain for resultant square printed dualband monopole antenna at (a) lower resonating band, and (b) higher resonating band

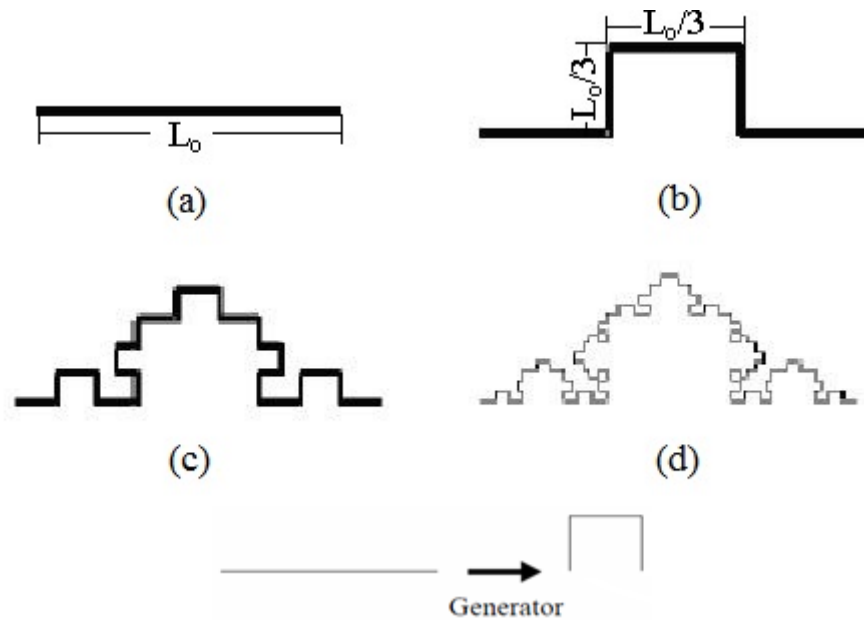


Figure.13. Minkowski fractal structure's generation mechanism; (a) the originator, (b) the first iteration, (c) the second iteration, and (d) the third iteration

The lower resonant frequency of the radiator is directly impacted by the internal slot length (L_s) besides the external radiator length (L_p), as shown in Fig. (9), and by the equations (5 and 6). In order to increase the electrical current channel between the radiator's two sides, an internal slot length (L_s) is inserted into the fractal structure. The resultant square printed monopole dualband antenna is represented in Figure 14 from the CST environment, which employs the Minkowski fractal geometry, for the first, second, and third iterations of the fractal (L_{s1} and L_{s2}). The antenna's center is located at the coordinates in the local coordinate system (0, 0, 0). (x , y , and z) There are three axes that go through the center of the object: width (X), length (Y), and thickness (Z). They are all orientated in the x -axis direction. Because the internal radiator length on both sides of the radiator is applied to the Minkowski space-filling fractal structure in the resulting dualband antenna, the internal length of the radiator is equal on both sides of the radiator. It is proven in Figure 14 that not only would the internal length of the antenna be varied, but the antenna's outer dimensions would be altered as well.

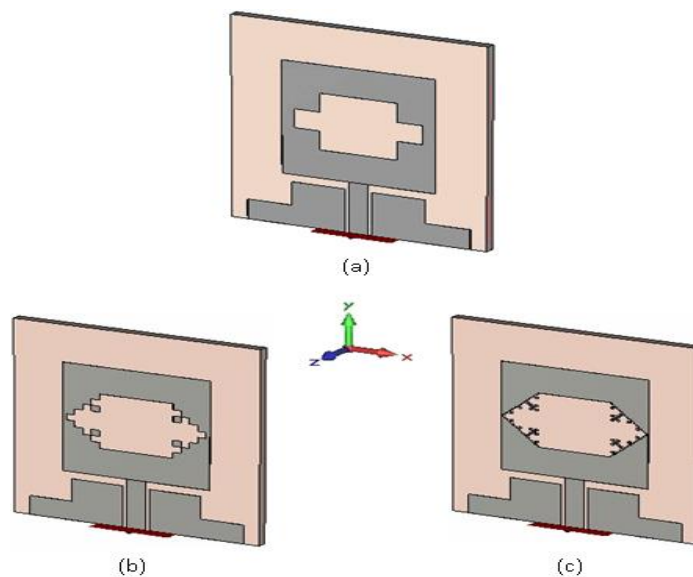


Figure 14. Local coordinates for the antenna's projected dual band square ring fractal antenna. for; (a) the first iteration, (b) the second iteration, and (c) the 3rd iteration

There are five segments in the first iteration, 25 segments in the second, and so on. A fractal structure's whole length at the n th iteration n , L_n is:

$$L_n = L_{n-1} + \frac{\sqrt{L_0}/3}{n} \quad \text{for } n \geq 1 \tag{7}$$

L_{n-1} stands for a preceding internal length (L_s) based on a fractal impact. At that point, an effective length (L_{eff}) could be modified to:

$$L_{eff} = L_n + 0.77L_p \tag{8}$$

When compared to a standard square slot antenna, the Minkowski space-filling fractal employs uneven radiating edges to lengthen the surface current path, consequential in a lower resonant frequency or a smaller antenna when the intended design frequency is maintained, as opposed to a standard square slot antenna.

Minkowski fractal structure is seen in its first, second, and third iterations, and its fourth and fifth iterations. As illustrated in Figure 15, the antenna's loss is caused by its square printed monopole design and the fact that it operates in two bands. Figure 15 depicts a frequency sweep from one to ten gigahertz to illustrate the return loss characteristics of the four antennas tested. In the absence of fractal structure, the dual-band monopole antenna developed here covers the 2.5/3.5 GHz WiMAX (Worldwide Interoperability for Microwave Access) frequency range and the 5.8 GHz WLAN frequency range in the lower resonant band from (2.64 – 3.55 GHz) in the lower resonant band (Wireless Local Area Network). Using the first iteration of the Minkowski space-filling fractal structure for (S11 10dB), this square printed monopole dual-band antenna can cover 2.5 GHz WiMAX and 5.8 GHz WLAN, respectively, in the lower resonance band from (2.46–3.36) and the higher resonance band from (5.44–6.92) GHz in the lower resonance band from (2.46–3.36) GHz.

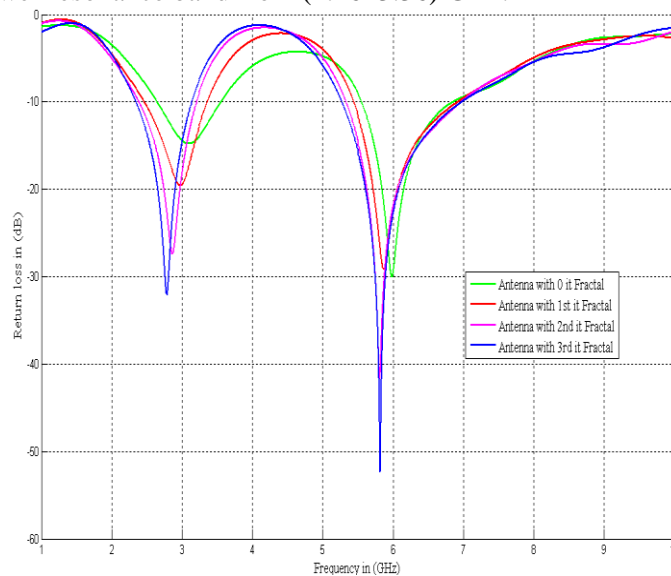


Figure-15. Impact of Minkowski fractal at first, second, and third iteration on the S11 parameter for consequential square printed monopole dualband antenna

Consider our second iteration Minkowski-space-filling fractal antenna: the lower resonance band from (2.39–3.2)GHz for WIMAX, (2.4–2.484 GHz WLAN, Bluetooth, ISM, and RFID; the upper resonance band covers 5.5 GHz WiMAX as well as 5.8 GHz WLAN, as well as ISM (Industrial Scientific Medical) and RFID; and the lower resonance band from (2.39–3.2)GHz covers Bluetooth, ISM, and RFID (Radio Frequency Identification). As a result of its Minkowski space-filling fractal design in its third iteration, the square printed monolithic dualband antenna with a lower resonance band from (2.35–3.13GHz) and a higher resonance range from (5.27–9GHz) can be used for both low and high-frequency applications. The two bands supported by this antenna, in other words, cover the entire spectrum of WiFi (Wireless Fidelity) applications, including lower and higher

WLAN, 2.5/5.5 GHz WIMAX, Bluetooth, ISM, and 2.45 GHz RFID (which all use frequencies between 2.4 and 2.484 GHz).

6. Conclusions

This paper describes how to use a modification technique and current distribution analysis on the UWB antenna's surface to successfully derive dualband response from the UWB response. Additional fractal geometry modifications have been made to the resulting antenna's radiating element to increase the antenna's dual-band performance. The CST MICROWAVE STUDIO finite integration approach simulator has been used to evaluate the antennas given. Antennas with dualband capabilities are feasibly employed in wireless communication applications because of their S11 input reflection coefficient (IRC). Antenna gains are near to omnidirectional for the two obtained bandwidths even though the antenna is small. Dual-band antenna responses may now be extracted from multi-band antennas without the need for filtering or modifying antenna size.

References

- [1] S. Behera and K. Vinoy. "Microstrip square ring antenna for dual-band operation," Progress In Electromagnetics Research, PIER 93, 41-56, 2009.
- [2] N. Behdad and K. Sarabandi. "A varactor-tuned dual-band slot antenna," IEEE Transactions on Antennas and Propagation, Vol. 54, No. 2, 401-408, 2006.
- [3] M. Alkanhal and A. Sheta. "A novel dual-band reconfigurable square-ring microstrip antenna," Prog. In Electromagnetics Research, PIER 70, 337-349, 2007.
- [4] A. Mishra, P. Singh, N. Yadav and J. Ansari. "Compact shorted microstrip patch antenna for dual-band operation," Progress In Electromagnetics Research, PIER C, Vol. 9, 171-182, 2009.
- [5] A. Ramadan, M. Al-Husseini, Y. Tawky, K. Kabalan, and A. El-Hajj. "A novel frequency/pattern-reconfigurable microstrip antenna for WLAN applications," Proceedings of the 4th European Conference on Antenna and Propagation, EuCAP, 2010.
- [6] W. Hu, Y. Yin, X. Yang, and X. Ren. "Compact printed antenna with h-shaped stub for dual-band operation," Electronic Lett., Vol. 46, No. 25, 2010.
- [7] J. Panda and R. Kshetrimayum. "A printed 2.4 GHz / 5.8 GHz dual-band monopole antenna with a protruding stub in the ground plane for WLAN and RFID applications," Progress In Electromagnetics Research, Vol. 117, 425-434, 2011.
- [8] W.-C. Liu. "Optimal design of dual-band CPW-fed G-shaped monopole antenna for WLAN application" Progress In Electromagnetics Research, PIER 74, 21-38, 2007.
- [9] D. Krishna, M. Gopikrishna, C. Aanandan, P. Mohanan, and K. Vasudevan. "Compact dual-band slot-loaded circular microstrip antenna with a superstrate," Progress In Electromagnetics Research, PIER 83, 245-255, 2008.
- [10] W. Hu, Y. Yin, S. Fan, J. Deng, and M. Zhang. "Compact CPW-fed square slot antenna for dual-band operation," Progress In Electromagnetics Research, Vol. 20, 165-173, 2011.
- [11] Y. Zhuo, L. Yan, X. Zhao, and K. Huang. "A compact dual-band patch antenna for WLAN applications," Progress In Electromagnetics Research, Vol. 26, 153-160, 2011.
- [12] C. Wang, Y. Lee, and K. Lee. "A dual-band CPW-fed L-slot Antenna with both linear and circular polarizations," Progress In Electromagnetics Research, PIER C, Vol. 21, 229-241, 2011.
- [13] Z. Aijaz and S. Shrivastava. "Aperture coupled microstrip slot antenna," IEEE International Conference on Recent Advances in Microwave Theory and Applications, Microwave 2008, Jaipur, India, 2008.
- [14] J. Ghalibafan and A. R. Attari. "A new dual-band microstrip antenna with U-shaped slot," Progress In Electromagnetics Research C, PIER C, Vol. 12, 215-223, 2010.
- [15] J. Ali. "A new dual-band E-shaped slot antenna design for wireless applications," Progress In Electromagnetics Research Symposium Proceedings, Suzhou, China, Sept. 12-16, 2011.

-
- [16] J. Ansari, P. Singh, and S. Dubey. "H-shaped stacked patch antenna for dual-band operation," *Progress In Electromagnetics Research B, PIER B*, Vol. 5, 291-302, 2008.
- [17] S. Gai, Y. Jiao, Y. Yang, C. Li and J. Gong. "Design of a novel microstrip-fed dual-band slot antenna for WLAN applications," *Progress In Electromagnetics Research*, Vol. 13, 75-81, 2010.
- [18] L. Kang, Y. Yin, H. Li, W. Huang, and S. Zheng. "Dual-wideband symmetrical G-shaped slotted monopole antenna for WLAN/ WiMAX applications," *Progress In Electromagnetics Research*, Vol. 17, 55-65, 2010.
- [19] J. Ali. "A new miniaturized fractal bandpass filter based on dual-mode microstrip square ring resonator," *Proceedings of the 5th International Multi-Conference on Signals, Systems, and Devices, IEEE SSD '08, Amman, Jordan*, 2008.
- [20] J. Ali and Y. Miz'el. "A new miniature Peano fractal-based bandpass filter design with second harmonic suppression," *3rd IEEE International Symposium on Microwave, Antenna, Propagation and EMC Technologies for Wireless Communications*, Beijing, China, 2009.
- [21] J. Ali and N. Hussain. "An extra reduced size dual-mode bandpass filter for wireless communication systems," *Proceedings of Progress in Electromagnetics Research Symposium, PIERS 2011, Suzhou, China*, 2011.
- [22] J. Ali, H. Alsaedi, M. Hasan and H. Hammas. "A Peano fractal-based dual-mode microstrip bandpass filters for wireless communication systems," *Proceedings of Progress in Electromagnetics Research Symposium, PIERS 2012, Moscow, Russia*, 2012.
- [23] J. Ali and H. Alsaedi. "Second-harmonic reduction of miniaturized dual-mode microstrip bandpass filters using fractal shaped open stub resonators," *Progress in Electromagnetics Research Symposium, PIERS 2012, KL, Malaysia*, 2012.
- [24] J. Ali, N. Hussain, A. Salim, H. Alsaedi. "A new tunable dual-mode bandpass filter design based on fractally slotted microstrip patch resonator," *Progress in Electromagnetics Research Symposium*, pp. 1225-1228, 2012.
- [25] Y. Mezaal, H. Eyyuboglu, J. Ali. "A novel design of two loosely coupled bandpass filters based on Hilbert-zz resonator with higher harmonic suppression," *Proc. IEEE 3rd International Conference on Advanced Computing and Communication Technologies, (ACCT)*, pp. 343-347, 2013.
- [26] Y. Mezaal, H. Eyyuboglu and J. Ali. "New dual-band dual-mode microstrip patch bandpass filter designs based on Sierpinski fractal geometry," *IEEE Third International Conference on Advanced Computing and Communication Technologies, ACCT*, pp. 348-352, Rohtak, India, 2013.
- [27] Y. Mezaal, H. Eyyuboglu, and J. Ali. "Wide bandpass and narrow bandstop microstrip filters based on Hilbert fractal geometry: design and simulation results," *PloS one*, 9: 1-12, 2014.
- [28] Y. Mezaal, H. Eyyuboglu and J. Ali. "New microstrip bandpass filter designs based on stepped impedance Hilbert fractal resonators," *IETE Journal of Research*. 60(3): 257-264, 2014.
- [29] Y. Mezaal, J. Ali and H. Eyyuboglu. "Miniaturised microstrip bandpass filters based on Moore fractal geometry," *International Journal of Electronics*, 102(8): 1306-1319, 2015.
- [30] J. Ali and H. Ziboon. "Design of compact bandpass filters based on fractal defected ground structure (DGS) resonators," *Indian Journal of Science and Technology*, 9: 1-9, 2016.
- [31] H. Ahmed, A. Salim, J. Ali, M. Alqaisy. "A fractal-based dual-mode microstrip bandstop filter for wireless applications," *Mediterranean Microwave Symposium*, 2017.
- [32] H. Ahmed, A. Salim, M. Hussan, H. Hammas, M. Yassen, S. Mutashar, J. Ali. "Design of compact dual-mode fractal-based microstrip band-reject filter," *ARNP Journal of Engineering and Applied Sciences*, 13(7): 2395- 2399, 2018.
- [33] Y. Mezaal, H. Eyyuboglu and J. Ali. "A new design of dual-band microstrip bandpass filter based on Peano fractal geometry: Design and simulation results," *13th IEEE Mediterranean Microwave Symposium, MMS'2013, Saida, Lebanon*, 2013.
-

-
- [34] M. Alqaisy, J. Ali, C. Chakrabarty, G. Hock. "Design of a compact dual-mode dual-band microstrip bandpass filter based on semi-fractal CSRR," Progress in Electromagnetics Research Symposium, 2013.
- [35] H. Ahmed, A. Salim, and J. Ali. "A Compact dual-band bandstop filter based on fractal microstrip resonators," Progress in Electromagnetics Research Symposium, PIERS 2015, Prague, Czech Republic, 2015.
- [36] M. Alqaisy, C. Chakrabarty, J. Ali and A. Alhawari. "A miniature fractal-based dual-mode dual-band microstrip bandpass filter design," International Journal of Microwave and Wireless Technologies. 7(2): 127-133, 2015.
- [37] H. Ahmed, A. Salim, J. Ali and N. Hussain. "A compact triple-band BSF design based on Minkowski fractal geometry," Proceedings of 18th IEEE Mediterranean Electrotechnical Conference, MELECON 2016, Limassol, Cyprus, 2016.
- [38] H. Ziboon and J. Ali. "Compact quad-band BPF design with a fractal stepped-impedance ring resonator," ARPN Journal of Engineering and Applied Sciences, 12(24): 7352-7363, 2017.
- [39] H. Ziboon and J. Ali. "Compact dual-band bandpass filter based on fractal stub-loaded resonator," Progress in Electromagnetics Research Symposium, St Petersburg, Russian Federation, 2017.
- [40] H. Ziboon and J. Ali. "Design of a triple-band fractal-based BPF with asymmetrical SLR structures," Journal of Engineering and Applied Sciences, 13(7), pp.1617-1620, 2018.
- [41] J. Ali, Z. AL-Hussain, A. Osman, and A. Salim. "A new compact size fractal-based microstrip slot antenna for GPS applications," Progress in Electromagnetics Research Symposium, PIERS, pp. 700-703, Kuala Lumpur, Malaysia, 2012.
- [42] J. Ali, A. Salim, A. Hammoodi, and H. Alsaedi. "An ultra-wideband printed monopole antenna with a fractal-based reduced ground plane," Progress in Electromagnetics Research Symposium. Moscow, Russia, 2012.
- [43] J. Ali and E. Ahmed. "A new fractal-based printed slot antenna for dual-band wireless communication applications," Progress in Electromagnetics Research Symposium, PIERS, pp. 1518-1521, Kuala Lumpur, Malaysia, 2012.
- [44] J. Ali, S. Abdulkareem, A. Hammoodi, A. Salim, M. Yassen, M. Hussan, and H. Al-Rizzo, "Cantor fractal-based printed slot antenna for dual-band wireless applications," International Journal of Microwave and Wireless Technologies, 8(2), pp.263-270, 2016.
- [45] S. Abdulkarim, A. Salim, J. Ali, A. Hammoodi, M. Yassen and M. Hassan. "A compact Peano-type fractal-based printed slot antenna for dual-band wireless applications," IEEE International RF and Microwave Conference, RFM, pp. 329-332, Penang, Malaysia, 2013.
- [46] J. Ali, M. Yassen, M. Hussan, and A. Salim. "A printed fractal-based slot antenna for multiband wireless communication applications," Progress in Electromagnetics Research Symposium, Moscow, Russia, 2012.
- [47] J. Ali. "A new microstrip-fed printed slot antenna based on Moore space-filling geometry," IEEE Loughborough Antennas and Propagation Conference, LAPC 2009, Loughborough, U.K, pp. 449-452, 2009.
- [48] P. Tilanthe, P. Sharma, and T. Bandopadhyay. "A compact UWB antenna with dual-band rejection," Progress In Electromagnetics Research, PIER B, Vol. 35, 389-405, 2011.